

Temperature dependence of anomalous Ettingshausen effect in SmCo₅-type permanent magnets at high temperatures

Asuka Miura¹, Keisuke Masuda¹, Takamasa Hirai¹, Ryo Iguchi¹, Takeshi Seki^{1,2,3},
Yoshio Miura^{1,4}, Hiroki Tsuchiura^{3,5}, Koki Takanashi^{2,3,6}, and Ken-ichi Uchida^{1,2,3,a)}

¹ National Institute for Materials Science, Tsukuba 305-0047, Japan.

² Institute for Materials Research, Tohoku University, Sendai 980-8577, Japan.

³ Center for Spintronics Research Network, Tohoku University, Sendai 980-8577, Japan.

⁴ Center for Spintronics Research Network, Osaka University, Osaka 560-8531, Japan.

⁵ Department of Applied Physics, Tohoku University, Sendai 980-8579, Japan.

⁶ Center for Science and Innovation in Spintronics, Core Research Cluster, Tohoku University, Sendai 980-8577, Japan.

^{a)} E-mail: UCHIDA.Kenichi@nims.go.jp

ABSTRACT

The anomalous Ettingshausen effect (AEE) in SmCo₅-type permanent magnets has been investigated in the high temperature range from room temperature to around 600 K. The anomalous Ettingshausen coefficient of the SmCo₅ and (SmGd)Co₅ magnets monotonically increases with increasing the temperature. Although AEE is almost independent of the Gd content around room temperature, the anomalous Ettingshausen coefficient of SmCo₅ is larger than that of (SmGd)Co₅ at high temperatures. The dimensionless figure of merit for AEE in SmCo₅ at high temperatures is much greater than the previous record obtained for the anomalous Nernst effect. The observed high temperature behavior of AEE is discussed based on the first-principles calculations of transverse transport coefficients.

The anomalous Ettingshausen effect (AEE) refers to the conversion of a charge current into a transverse heat current in a magnetic conductor. The AEE-induced heat current density is described as

$$\mathbf{j}_{q,AEE} = \Pi_{AEE} (\mathbf{j}_c \times \mathbf{m}), \quad (1)$$

where \mathbf{j}_c , \mathbf{m} , and Π_{AEE} denote the charge current density, unit vector of magnetization, and anomalous Ettingshausen coefficient, respectively [Fig. 1(a)].¹⁻¹⁰ Since AEE works as temperature modulators with simple structure and versatile scaling owing to the unique thermoelectric conversion symmetry, it may pave the way for thermal management technologies for electronic and spintronic devices. Experimental studies on AEE have been developed rapidly since the establishment of the versatile measurement technique for this phenomenon.⁴

Recently, large AEE was observed in SmCo₅-type permanent magnets at room temperature.⁸ This result indicates that SmCo₅-type magnets also exhibit good performance for the thermoelectric generation based on the anomalous Nernst effect (ANE),¹¹⁻²⁶ which is the Onsager reciprocal of AEE. The figure of merit for AEE/ANE in SmCo₅-type magnets at room temperature is comparable to the record-high value in a Heusler ferromagnet.¹⁹ In addition to the thermoelectric conversion performance, permanent magnets have several practical advantages over soft magnetic materials for AEE/ANE applications. First, in permanent magnets, AEE/ANE works in the absence of magnetic fields and its performance is not affected by external field disturbance. Second, permanent magnets are mass-produced and widely distributed in a society, enabling the construction of ubiquitous, low-cost, and large-area

AEE/ANE devices. Therefore, clarifying the thermoelectric conversion performance of AEE/ANE in SmCo₅-type magnets is important.

In this study, we report the observation of AEE in SmCo₅-type magnets in the high temperature range from room temperature to around $T = 600$ K. We focus on this temperature range because of the working temperature limit of SmCo₅-type magnets; as shown in Fig. 1(b), the remanent magnetization M_r of the SmCo₅-type magnets sharply decreases around 700 K. The previous study shows that, although the SmCo₅-type magnets with different Gd contents have substantially different saturation magnetization M_s and microstructures, the transport properties are almost independent of the composition at room temperature.⁸ However, the behaviors of AEE at high temperatures are yet to be clarified.

The samples used in this study are polycrystalline SmCo₅ and (SmGd)Co₅ slabs with a rectangular cuboid shape, commercially available from Magfine Corporation, Japan. The Sm:Gd ratio in the (SmGd)Co₅ slab is 48:52 in at%. To estimate the figure of merit for AEE and the Seebeck effect in the SmCo₅ and (SmGd)Co₅ slabs, we measured the T dependence of Π_{AEE} , the longitudinal electrical conductivity σ_{xx} , thermal conductivity κ , and Seebeck coefficient S_{xx} . The sample size for the measurements of Π_{AEE} , σ_{xx} , and S_{xx} (κ) is 10.0 or $12.0 \times 1.5 \times 1.5$ mm³ ($10.0 \times 10.0 \times 2.0$ mm³), where the samples are magnetized along the 1.5 mm (10.0 mm) direction in the absence of magnetic fields. AEE was measured by means of the lock-in thermography (LIT) technique,^{4-10,27-29} as detailed below. The T dependence of σ_{xx} and S_{xx} was simultaneously measured with the Seebeck coefficient/electric resistance measurement system (ZEM-3, ADVANCE RIKO, Inc). The T dependence of κ was determined through thermal diffusivity measured by the laser flash method, specific heat measured by the differential scanning calorimetry, and density measured by the Archimedes method.

The procedures for the AEE measurements are as follows. The LIT method allows us to estimate Π_{AEE} of permanent magnets without applying external magnetic fields, when M_r is finite.⁸ We measured thermal images of the surface of the SmCo₅ or (SmGd)Co₅ slab with an infrared camera while applying a square-wave-modulated AC charge current with the frequency f , amplitude J_c (with the density j_c), and zero offset to the slab in the x direction and extracted the first harmonic response of the detected images, which are transformed into the lock-in amplitude A and phase ϕ images through Fourier analysis [Fig. 1(f)]. Based on this procedure, thermoelectric signals ($\propto J_c$) free from Joule-heating signals ($\propto J_c^2$) can be detected.⁴⁻¹⁰ The thermoelectric signals around the center of the sample are due purely to AEE, which are separated from parasitic signals due to the Peltier effect generated at the ends of the sample. The sample was fixed on a sapphire substrate attached to the top of a Cu stage of which the temperature can be tuned with a heater and a resistance temperature sensor embedded in the stage [Fig. 1(f)]. To enhance the infrared emissivity, the top surface of the sample was coated with insulating black ink. The LIT measurements were performed in a high vacuum and thermal images were monitored through an infrared-transparent CaF₂ window. The effect of the CaF₂ window to the thermal images was calibrated by comparing the infrared intensity on the surface of a reference thermometer, measured with the infrared camera through the window, and the output of the thermometer. This calibration allows us to monitor the sample temperature during the LIT measurements through steady-state thermal images [Fig. 1(e)]. Figures 1(c) and 1(d) respectively show an example of the A and ϕ images for the SmCo₅ slab at $T = 317$ K, where the remanent magnetization (charge current) is along the z (x) direction. Clear current-induced temperature modulation was observed to appear on the entire surface of the slab. This behavior is consistent with the symmetry of AEE; the temperature modulation signal is generated as a result of the AEE-induced heat current along the y direction [Fig. 1(a)].

Figure 2(a) shows the T dependence of A/j_c for the SmCo₅ and (SmGd)Co₅ slabs at $f = 10$ Hz, where the data points were obtained by averaging the temperature modulation signals

on the area defined by the white rectangle with a size of 100×40 pixels in Fig. 1(e). The AEE-induced temperature modulation appears in both the slabs in the whole temperature range studied without changing its sign [see the inset to Fig. 2(a)].

For the quantitative discussion, we estimated the magnitude of the AEE-induced temperature modulation in the steady state, *i.e.*, at $f=0$ Hz, by fitting the f dependence of the AEE signal with the solution of the heat equation in the frequency domain [see Fig. 2(b) and Ref. 8 for details]. From the steady-state AEE signal, we can determine the anomalous Ettingshausen coefficient as $\Pi_{\text{AEE}} = \kappa \Delta T / \tilde{j}_c L$, where \tilde{j}_c , ΔT , and L are the sinusoidal amplitude of the charge current density, temperature difference between the top and bottom surfaces of the slab, and thickness of the slab ($= 1.5$ mm), respectively. Here, recall the fact that the magnetization of the SmCo₅ and (SmGd)Co₅ slabs was not fully saturated during the AEE measurements [Fig. 1(b)]. We thus set $\Delta T = 2A_{0\text{Hz}}(M_s/M_r)$ to take the T -dependent difference between M_r and M_s into consideration, where $A_{0\text{Hz}}$ denotes A at $f=0$ Hz. We can obtain the anomalous Nernst coefficient S_{ANE} via the Onsager reciprocal relation: $\Pi_{\text{AEE}} = S_{\text{ANE}}T$.

In Fig. 3(a), we show the T dependence of Π_{AEE} for SmCo₅ and (SmGd)Co₅. Around room temperature, Π_{AEE} of SmCo₅ is comparable to that of (SmGd)Co₅, consistent with the previous result showing the weak dependence of AEE on the Gd content in the SmCo₅-type magnets.⁸ We found that Π_{AEE} monotonically increases with increasing T for both the slabs and Π_{AEE} of SmCo₅ is larger than that of (SmGd)Co₅ at high temperatures. The corresponding S_{ANE} values are shown in Fig. 3(b); S_{ANE} also monotonically increases with T but its T dependence is much weaker than that of Π_{AEE} due to the factor T in the Onsager reciprocal relation. The maximum Π_{AEE} (S_{ANE}) value for SmCo₅ is 3.2×10^{-3} V (5.6×10^{-6} VK⁻¹) at $T = 572$ K. We confirmed negative (no) correlation between S_{ANE} and M_s for SmCo₅ [(SmGd)Co₅], which clearly deviates from the scaling behavior reported in Ref. 16 [see the inset to Fig. 3(b)].

Figures 3(c) shows the T dependence of the dimensionless figure of merit for AEE/ANE in the SmCo₅ and (SmGd)Co₅ slabs, which was estimated based on the following definition:^{8,30}

$$Z_{\text{AEE}}T = \frac{\Pi_{\text{AEE}}^2 \sigma_{xx}}{\kappa} \frac{1}{T} \quad \left(= \frac{S_{\text{ANE}}^2 \sigma_{xx}}{\kappa} T \right). \quad (2)$$

By using the T dependence of Π_{AEE} [Fig. 3(a)] together with σ_{xx} and κ [Fig. 3(d)], we obtained the $Z_{\text{AEE}}T$ values. Although the T -dependent increase of Π_{AEE} is partially offset by the T -dependent decrease of σ_{xx} and the factor $1/T$ in Eq. (2), the resulting $Z_{\text{AEE}}T$ monotonically increases with T for both the slabs. The estimated $Z_{\text{AEE}}T$ value for SmCo₅ is 0.5×10^{-3} (1.1×10^{-3}) at $T = 317$ K (572 K). Significantly, the $Z_{\text{AEE}}T$ value at the high temperature marks a record high for AEE/ANE, which is much higher than the value of full-Heusler Co₂MnGa.¹⁹ We also note that even the maximum $Z_{\text{AEE}}T$ value for SmCo₅ is one order of magnitude smaller than the figure of merit for the Seebeck effect $Z_{\text{SE}}T$ [Figs. 3(c) and 3(f)], which is due to the fact that $|S_{\text{ANE}}|$ is several times smaller than $|S_{xx}|$ [Figs. 3(b) and 3(e)].

We are now in a position to discuss the observed T dependence of AEE/ANE in SmCo₅. The following discussion is mainly presented in terms of ANE because of the simple notation. In general, the anomalous Nernst coefficient can be divided into the two terms:²⁴

$$S_{\text{ANE}} = \rho_{xx}\alpha_{xy} + \rho_{xy}\alpha_{xx} \equiv S_{\text{I}} + S_{\text{II}}, \quad (3)$$

where $\rho_{xx} = 1/\sigma_{xx}$ ($\rho_{xy} = -\sigma_{xy}/\sigma_{xx}^2$) denotes the diagonal (off-diagonal) component of the electrical resistivity tensor, α_{xx} (α_{xy}) the diagonal (off-diagonal) component of the thermoelectric conductivity tensor, $S_{\text{I}} = \rho_{xx}\alpha_{xy} = \alpha_{xy}/\sigma_{xx}$, and $S_{\text{II}} = \rho_{xy}\alpha_{xx} = -S_{xx}\sigma_{xy}/\sigma_{xx}$. The S_{I} term is an intrinsic part of ANE as it originates from the transverse thermoelectric conductivity α_{xy} , which is determined by the energy derivative of the anomalous Hall conductivity σ_{xy} . In

contrast, the S_{II} term is attributed to the concerted action of the Seebeck and anomalous Hall effects. In Ref. 8, we showed that AEE/ANE in the SmCo₅-type magnets at room temperature originates mainly from the S_I term owing to the large α_{xy} and the experimental results are well reproduced by the first-principles calculations of the transverse transport coefficients. To investigate the S_I and S_{II} contributions at high temperatures, we compare the experimental results with the first-principles calculations based on the same procedures shown in Ref. 8. Here, we calculated σ_{xy} and α_{xy} of SmCo₅ with changing T and the chemical potential μ , where the electronic band structure at absolute zero temperature is assumed and the T -dependent effects are included through the Fermi distribution function. By combining the calculated α_{xy} (σ_{xy}) values with the observed σ_{xx} (S_{xx} and σ_{xx}) values for SmCo₅, we estimated the S_I (S_{II}) contribution.

Figures 4(a) and 4(b) show the μ dependence of σ_{xy} and α_{xy} for SmCo₅ at various temperatures, respectively. At $\mu = 0$ eV, the calculated α_{xy} shows large values of $> 6 \text{ Am}^{-1}\text{K}^{-1}$ and monotonically increases with increasing T , while σ_{xy} is very small above room temperature. As shown in Fig. 4(c), the calculated T dependence of S_{ANE} at $\mu = 0$ eV is dominated by the S_I contribution, and the S_{II} values are negligibly small. In this case, the calculation cannot explain the high temperature behavior of AEE/ANE; the difference between the observed and calculated S_{ANE} values increases with T . The discrepancy between ANE experiments and first-principles calculations often occurs, but it has been reported that the experimental results can be explained by considering the μ shift due to carrier doping.^{21,26} We thus adopted a similar strategy; by comparing the experimental and calculated results with changing μ , we found that the calculation at around $\mu = -0.14$ eV well reproduces the observed T dependence of S_{ANE} for SmCo₅ over the T range of interest, where the S_I (S_{II}) contribution at $\mu = -0.14$ eV is smaller (larger) than that at $\mu = 0$ eV [Fig. 4(c)]. We also note that the calculated ratio between S_I and S_{II} at $\mu = -0.14$ eV is quantitatively consistent with the experimental results at room temperature.⁸ These results suggest that the high temperature behavior of AEE/ANE for SmCo₅ is attributed to its intrinsic band structure and μ shift, where the hole doping of $\mu = -0.14$ eV corresponds to a change in the number of valence electrons of 1.32 per a SmCo₅ unit cell. Nevertheless, to confirm the validity of this interpretation and clarify the carrier-doping effects, systematic measurements of the composition and/or impurity dependences of AEE/ANE in the SmCo₅-type magnets and direct observation of their band structures are necessary.

In conclusion, we have investigated the transport properties in the SmCo₅-type permanent magnets and observed large AEE above room temperature. The anomalous Ettingshausen coefficient of the SmCo₅ and (SmGd)Co₅ magnets monotonically increases with increasing the temperature. The SmCo₅ magnet shows larger AEE at high temperatures, while both the magnets exhibit comparable AEE signals around room temperature. The dimensionless figure of merit for AEE in SmCo₅ reaches $\sim 1 \times 10^{-3}$ when $T > 500$ K, which is the maximum value reported so far. The temperature dependence of AEE in SmCo₅ can be explained by the first-principles calculations typically used for estimating the intrinsic contribution of AEE/ANE if the chemical potential shift is taken into account. These results provide a crucial piece of information for understanding the microscopic mechanism of AEE/ANE in the SmCo₅-type magnets and for creating thermoelectric converters based on permanent magnets.

The authors thank Y. Sakuraba for valuable discussions. This work was supported by CREST “Creation of Innovative Core Technologies for Nano-enabled Thermal Management” (JPMJCR17I1) from JST, Japan, Grant-in-Aid for Scientific Research (S) (JP18H05246) and Grant-in-Aid for Scientific Research (B) (JP19H02585) from JSPS KAKENHI, Japan, and the Canon Foundation. A.M. and T.H. are supported by JSPS through Research Fellowship for Young Scientists (JP18J02115, JP20J00365).

REFERENCES

- ¹ P. W. Bridgman, Phys. Rev. **24**, 644 (1924).
- ² E. H. Hall, Phys. Rev. **26**, 820 (1925).
- ³ E. H. Butler Jr. and E. M. Pugh, Phys. Rev. **57**, 916 (1940).
- ⁴ T. Seki, R. Iguchi, K. Takanashi, and K. Uchida, Appl. Phys. Lett. **112**, 152403 (2018).
- ⁵ K. Uchida, S. Daimon, R. Iguchi, and E. Saitoh, Nature **558**, 95 (2018).
- ⁶ T. Seki, R. Iguchi, K. Takanashi, and K. Uchida, J. Phys. D: Appl. Phys. **51**, 254001 (2018).
- ⁷ R. Das, R. Iguchi, and K. Uchida, Phys. Rev. Appl. **11**, 034022 (2019).
- ⁸ A. Miura, H. Sepehri-Amin, K. Masuda, H. Tsuchiura, Y. Miura, R. Iguchi, Y. Sakuraba, J. Shiomi, K. Hono, and K. Uchida, Appl. Phys. Lett. **115**, 222403 (2019).
- ⁹ R. Modak and K. Uchida, Appl. Phys. Lett. **116**, 032403 (2020).
- ¹⁰ A. Miura, R. Iguchi, T. Seki, K. Takanashi, and K. Uchida, Phys. Rev. Mater. **4**, 034409 (2020).
- ¹¹ T. Miyasato, N. Abe, T. Fujii, A. Asamitsu, S. Onoda, Y. Onose, N. Nagaosa, and Y. Tokura, Phys. Rev. Lett. **99**, 086602 (2007).
- ¹² M. Mizuguchi, S. Ohata, K. Uchida, E. Saitoh, and K. Takanashi, Appl. Phys. Express **5**, 093002 (2012).
- ¹³ Y. Sakuraba, K. Hasegawa, M. Mizuguchi, T. Kubota, S. Mizukami, T. Miyazaki, and K. Takanashi, Appl. Phys. Express **6**, 033003 (2013).
- ¹⁴ R. Ramos, M. H. Aguirre, A. Anadón, J. Blasco, I. Lucas, K. Uchida, P. A. Algarabel, L. Morellón, E. Saitoh, and M. R. Ibarra, Phys. Rev. B **90**, 054422 (2014).
- ¹⁵ K. Hasegawa, M. Mizuguchi, Y. Sakuraba, T. Kamada, T. Kojima, T. Kubota, S. Mizukami, T. Miyazaki, and K. Takanashi, Appl. Phys. Lett. **106**, 252405 (2015).
- ¹⁶ K. Uchida, T. Kikkawa, T. Seki, T. Oyake, J. Shiomi, Z. Qiu, K. Takanashi, and E. Saitoh, Phys. Rev. B **92**, 094414 (2015).
- ¹⁷ M. Ikhlas, T. Tomita, T. Koretsune, M. Suzuki, D. Nishio-Hamane, R. Arita, Y. Otani, and S. Nakatsuji, Nat. Phys. **13**, 1085 (2017).
- ¹⁸ Z. Yang, E. A. Codecido, J. Marquez, Y. Zheng, J. P. Heremans, and R. C. Myers, AIP Adv. **7**, 095017 (2017).
- ¹⁹ A. Sakai, Y. P. Mizuta, A. A. Nugroho, R. Sihombing, T. Koretsune, M. Suzuki, N. Takemori, R. Ishii, D. Nishio-Hamane, R. Arita, P. Goswami, and S. Nakatsuji, Nat. Phys. **14**, 1119 (2018).
- ²⁰ H. Reichlova, R. Schlitz, S. Beckert, P. Swekis, A. Markou, Y.-C. Chen, D. Kriegner, S. Fabretti, G. H. Park, A. Niemann, S. Sudheendra, A. Thomas, K. Nielsch, C. Felser, and S. T. B. Goennenwein, Appl. Phys. Lett. **113**, 212405 (2018).
- ²¹ S. N. Guin, K. Manna, J. Noky, S. J. Watzman, C. Fu, N. Kumar, W. Schnelle, C. Shekhar, Y. Sun, J. Gooth, and C. Felser, NPG Asia Mater. **11**, 16 (2019).
- ²² H. Nakayama, K. Masuda, J. Wang, A. Miura, K. Uchida, M. Murata, and Y. Sakuraba, Phys. Rev. Mater. **3**, 114412 (2019).
- ²³ G.-H. Park, H. Reichlova, R. Schlitz, M. Lammel, A. Markou, P. Swekis, P. Ritzinger, D. Kriegner, J. Noky, J. Gayles, Y. Sun, C. Felser, K. Nielsch, S. T. B. Goennenwein, and A. Thomas, Phys. Rev. B **101**, 060406(R) (2020).
- ²⁴ Y. Sakuraba, K. Hyodo, A. Sakuma, and S. Mitani, Phys. Rev. B **101**, 134407 (2020).
- ²⁵ A. Sakai, S. Minami, T. Koretsune, T. Chen, T. Higo, Y. Wang, T. Nomoto, M. Hirayama, S. Miwa, D. Nishio-Hamane, F. Ishii, R. Arita, and S. Nakatsuji, Nature **581**, 53 (2020).
- ²⁶ K. Sumida, Y. Sakuraba, K. Masuda, T. Kono, M. Kakoki, K. Goto, K. Miyamoto, Y. Miura, T. Okuda, and A. Kimura, e-print arXiv:2006.15769.
- ²⁷ O. Breitenstein, W. Warta, and M. Langenkamp, *Lock-in thermography: Basics and Use for Evaluating Electronic Devices and Materials Introduction*. (Springer, Berlin/Heidelberg, Germany, 2010).
- ²⁸ O. Wid, J. Bauer, A. Müller, O. Breitenstein, S. S. P. Parkin, and G. Schmidt, Sci. Rep. **6**, 28233 (2016).
- ²⁹ S. Daimon, R. Iguchi, T. Hioki, E. Saitoh, and K. Uchida, Nat. Commun. **7**, 13754 (2016).
- ³⁰ K. Uchida, H. Adachi, T. Kikkawa, A. Kirihaara, M. Ishida, S. Yorozu, S. Maekawa, and E. Saitoh, Proc. IEEE **104**, 1946 (2016).

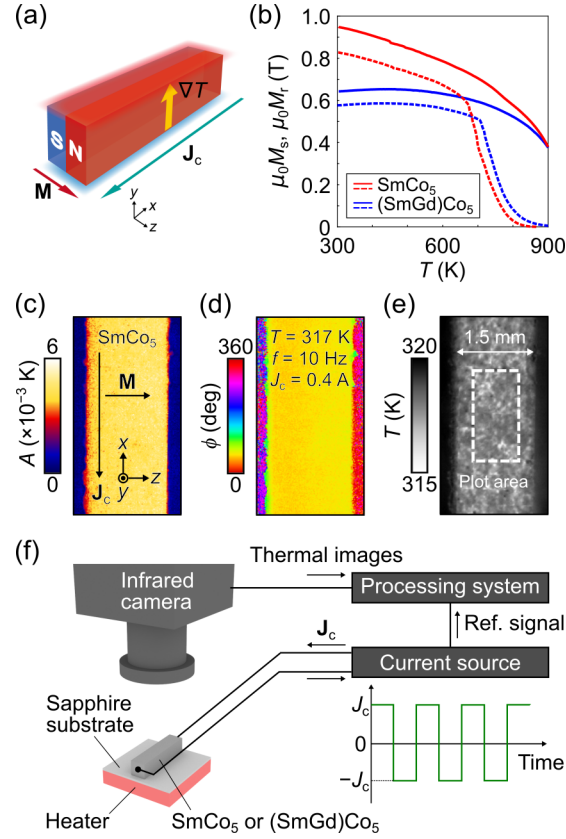


FIG. 1. (a) Schematic illustration of AEE in a permanent magnet in the in-plane magnetized configuration. \mathbf{J}_c , ∇T , and \mathbf{M} denote the charge current applied to the magnet, temperature gradient generated as a result of AEE, and direction of the remanent magnetization, respectively. (b) Temperature T dependence of the saturation magnetization $\mu_0 M_s$ (solid lines) and the remanent magnetization $\mu_0 M_r$ (dotted lines) for the SmCo_5 and $(\text{SmGd})\text{Co}_5$ slabs, measured by the vibrating sample magnetometry. μ_0 is the vacuum permeability. (c) and (d) Lock-in amplitude A and phase ϕ images for the SmCo_5 slab at $T = 317$ K, $f = 10$ Hz, and $J_c = 0.4$ A. f and J_c denote the frequency and amplitude of the square-wave-modulated charge current, respectively. (e) Steady-state thermal image for the SmCo_5 slab with the black-ink coating. (f) Schematic illustration of AEE measurements based on LIT. The measurements were performed in the absence of an external magnetic field. The heater and resistance temperature sensor embedded in the Cu stage were used for controlling the sample temperature.

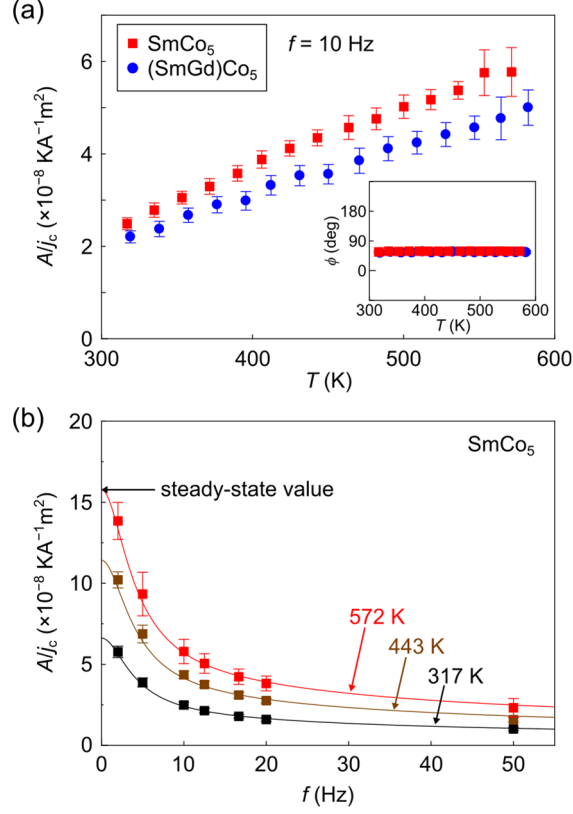


FIG. 2. (a) T dependence of A/j_c for the SmCo_5 (red squares) and $(\text{SmGd})\text{Co}_5$ (blue circles) slabs at $f = 10 \text{ Hz}$. j_c denotes the amplitude of the square-wave-modulated charge current density. The inset shows the T dependence of ϕ . The error bars represent the standard deviation of the A/j_c values on the area defined by the white rectangle with a size of 100×40 pixels in Fig. 1(e). (b) f dependence of A/j_c for the SmCo_5 slab at $T = 317 \text{ K}$ (black), 443 K (brown), and 572 K (red). The solid lines show the calculated f dependence of A/j_c for the SmCo_5 slab, obtained by solving the one-dimensional heat equation. The calculation procedures are shown in Ref. 8.

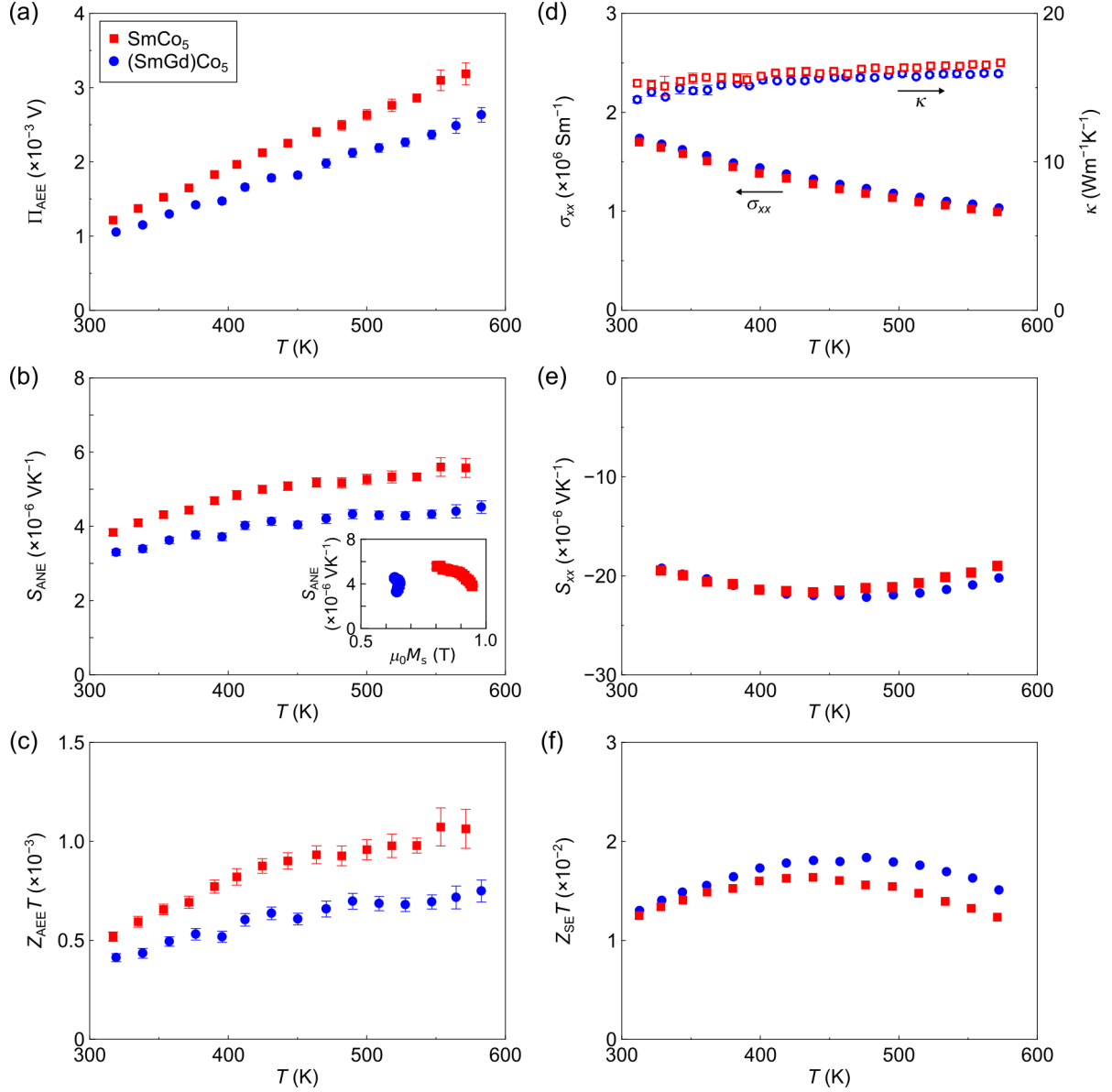


FIG. 3. (a) and (b) T dependence of the anomalous Ettingshausen coefficient Π_{AEE} and the anomalous Nernst coefficient $S_{\text{ANE}} (= \Pi_{\text{AEE}}/T)$ for SmCo_5 (red squares) and $(\text{SmGd})\text{Co}_5$ (blue circles). The inset to (b) shows the $\mu_0 M_s$ dependence of S_{ANE} . (c) T dependence of the dimensionless figure of merit $Z_{\text{AEE}} T$ for AEE. (d) T dependence of the longitudinal electrical conductivity σ_{xx} (closed) and the thermal conductivity κ (open). (e) and (f) T dependence of the Seebeck coefficient S_{xx} and the dimensionless figure of merit $Z_{\text{SE}} T$ for the Seebeck effect.

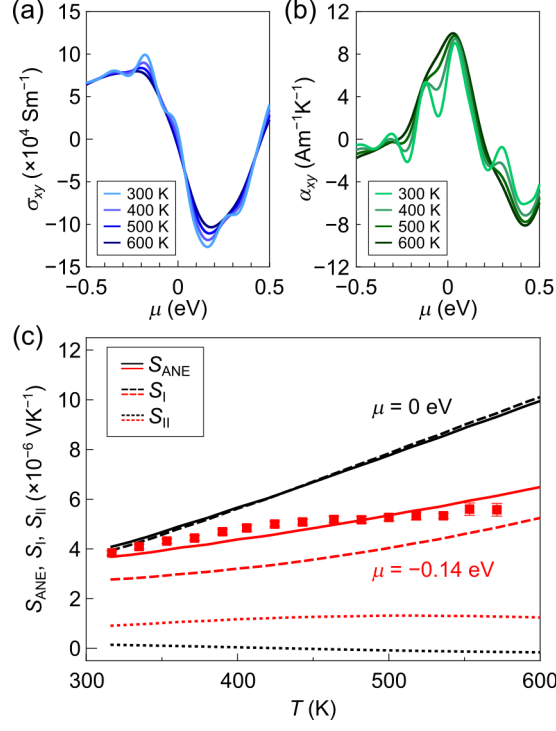


FIG. 4. (a) and (b) Chemical potential μ dependence of the anomalous Hall conductivity σ_{xy} and the transverse thermoelectric conductivity α_{xy} of SmCo_5 for various values of T , obtained from the first-principles calculations. The calculation procedures are shown in Ref. 8. (c) Comparison of the T dependence of the experimentally observed S_{ANE} values (red squares) with that of S_{ANE} (solid lines), S_{I} (dashed lines), and S_{II} (dotted lines) estimated based on the first-principles calculations for SmCo_5 . The black (red) lines show the calculated results for $\mu = 0$ eV (-0.14 eV).